Moving average process underlying the holographic–optical–tweezers experiments

Jakub Ślęzak,* Sławomir Drobczyński, Karina Weron, and Jan Masajada

Wrocław University of Technology, Wyb. Wyspiańskiego 27, 50-370 Wrocław, Poland

*Corresponding author: jakub.slezak@pwr.edu.pl

Received 5 November 2013; revised 3 February 2014; accepted 9 February 2014;
posted 18 February 2014 (Doc. ID 200775); published 21 March 2014

We study the statistical properties of recordings that contain time-dependent positions of a bead trapped in optical tweezers. Analysis of such a time series indicates that the commonly accepted model, i.e., the autoregressive process of first-order, is not sufficient to fit the data. We show the presence of a first-order moving average part in the dynamical model of the system. We explain the origin of this part as an influence of the high-frequency CCD camera on the measurements. We show that this influence evidently depends on the applied exposure time. The proposed autoregressive moving average model appears to reflect perfectly all statistical features of the high-frequency recording data. © 2014 Optical Society of America

OCIS codes: (000.3860) Mathematical methods in physics; (350.4855) Optical tweezers or optical manipulation; (140.7010) Laser trapping; (170.4520) Optical confinement and manipulation.
http://dx.doi.org/10.1364/AO.53.00B254

1. Introduction

Optical tweezers are a versatile tool, which allows for the manipulation of micrometer-sized particles noninvasively, and to measure forces even on the pico-Newton scale [1–3]. For these reasons, they have a wide range of applications in many fields of biology and soft condensed matter physics, including, e.g., stretching of DNA and other polymers [4,5], molecular motors research [6,7], and the analysis of colloidal suspensions [8]. Optical tweezers technology is now extensively developed and its applications multiply, so the need for improved methods of calibration is growing. The physics of the simplest situations, like the motion of a trapped bead in water, is well-known; however, studies of more complex environments require a thorough understanding of the experimental data. In these newly developed areas, the measurements performed using a CCD camera are especially useful, because the camera provides a great deal of diverse information and allows for the tracking of many objects simultaneously. As shown in our analysis below, in the case of high-frequency measurements, the camera has a significant influence on the measurements.

To explain this phenomenon, we start by recalling briefly the classical Einstein theory of the optical tweezers. A trajectory $t \mapsto X(t)$ of a colloidal particle trapped in a viscous fluid by optical tweezers is a solution of the equation of the force balance [9]

$$0 = F_S + F_O + F_T, \tag{1}$$

where

- $F_S = -\beta(\mathrm{d}X/\mathrm{d}t)$ is the Stokes force (friction of liquid) acting on the spherical bead with radius r within the liquid with viscosity η, $\beta = 6\pi\eta r$;
- $F_O = -k_h X$ is the force caused by the optical tweezers; we use harmonic approximation, i.e., assume the potential is harmonic with stiffness k_h;
- $F_T = \sqrt{k_B T \beta}\mathrm{d}B/\mathrm{d}t$ is the thermal force: it models the exchange of momenta with particles of the liquid; B is the Wiener process, i.e., the trajectory

1559-128X/14/10B254-05$15.00/0

of a free Brownian particle (k_B denotes Boltzmann constant).

Substitution of the explicit formulas assures that the above force balance condition is equivalent to the following stochastic differential equation

$$\mathrm{d}X = -\mathrm{d}t \cdot \lambda X + D\mathrm{d}B, \tag{2}$$

where $\lambda = k_h/\beta$ and $D = \sqrt{k_B T/\beta}$. Its stationary solution is known as the Ornstein–Uhlenbeck process [10]

$$X(t) = D\int_{-\infty}^{t} \mathrm{d}B(s)\mathrm{e}^{-(t-s)\lambda}. \tag{3}$$

As we see, a position of the bead is expressed as a convolution of the changes of momenta $\mathrm{d}B$ with the exponential function.

2. Recorded Data

The measurements (see Fig. 1) were performed with holographic optical tweezers [11,12]. Our tweezers were built on the biological Olympus IX71 microscope with a holographic system added for optical traps generation. As a light source we used single mode laser diode ($\lambda = 980$ nm, $\mathrm{P_{max}} = 450$ mW). The diode was single-mode pigtail fiber with NA = 0.14 and stabilized by fiber Bragg grating. The holograms were written on the spatial light modulator (SLM) HoloEye PLUTO_NIR and reconstructed by the microscope at the sample plane. All recordings were obtained using high-speed camera MC1362 (Mikrotron GmbH), CameraLink, CMOS sensor, 1280×1024. The photos of the bead were taken in 150×160 pixels resolution taken with exposure time 45 μs. The position of the bead was determined as a mass center of the recoded image [13]. Single analyzed time series consisted of up to 6×10^4 frames taken with a sampling frequency up to 10^4 fps. The test liquid was pure water.

3. Sampling Process

The data obtained during processing of the recorded frames are given in the form of a sequence of the bead's positions taken with a constant frequency. Instead of the continuous process $X(t)$, we observe sampled process X_n as

$$X_n := X(n\Delta t), \qquad n \in \{0, 1, 2, \ldots\}, \Delta t = \text{const}. \tag{4}$$

Here, Δt is the interval between measurements, the inverse of the sampling frequency. By direct calculation, one can confirm that the sampled Ornstein–Uhlenbeck process has the property

$$X_n = aX_{n-1} + \xi_n, \tag{5}$$

where $a = \mathrm{e}^{-\lambda\Delta t}$ is a constant and

$$\xi_n = D\int_{n\Delta t}^{n\Delta t+\Delta t} \mathrm{d}B(s)\mathrm{e}^{-\lambda(n\Delta t - s)}. \tag{6}$$

The above formula implies that all ξ_n are mutually independent Gaussian random variables with a mean $\mu = 0$ and variance $\sigma^2 = (D^2/2\lambda)(\mathrm{e}^{2\lambda\Delta t} - 1)$; in other words, the sequence of ξ_n is the Gaussian white noise. Any process of type (5), for which the present value X_n is a linear combination (regression) of the past values and some external noise, is called an autoregressive process, denoted AR. Here, the present value depends explicitly on one past value X_{n-1}, so we call it AR of first-order, denoted AR(1) [14]. The coefficient a and, consequently, stiffness k_h, can be estimated using classical regression with the sequence of X_n taken as a variable y and shifted sequence of X_{n-1} taken as a variable x. The well-known least squares estimator of the slope in this case reads [12]

$$\hat{a} = \frac{\sum_i X_i X_{i-1}}{\sum_i X_i^2}. \tag{7}$$

To study the properties of the AR(1) process we can express X_n as a function of ξ_n, using formula (5) recursively:

$$\begin{aligned} X_n &= a^2 X_{n-2} + \xi_n + a\xi_{n-1} \\ &= a^{k+1}X_{n-k-1} + \xi_n + a\xi_{n-1} + \cdots + a^k\xi_{n-k}. \end{aligned} \tag{8}$$

The terms $a^{k+1}X_{n-k-1}$ diminish with growing k because $a < 1$, so we may write

$$X_n = \sum_{k=0}^{\infty} a^k \xi_{n-k}. \tag{9}$$

Note that the variables ξ_{n-k} for $n - k < 0$ are not observed, because the measurement starts at time zero. Directly from this formula, a type of memory present in the analyzed time series can be deduced. The memory of the process is usually characterized by the autocovariance function, which is defined as

$$\mathrm{acov}_X(i,j) := \mathrm{cov}(X_i, X_j). \tag{10}$$

For a stationary process the autocovariance depends only on a difference of the times: $\mathrm{acov}_X(i,j) = \mathrm{acov}_X(k = i - j)$. Using the identity $\mathrm{cov}(\xi_i, \xi_j) = \delta_{i,j}$, directly from (9) we obtain that, for the AR(1) process

$$\mathrm{acov}_X(k) = \frac{\sigma^2}{1 - a^{-2}} a^{-|k|}. \tag{11}$$

It is a geometric sequence and geometrically decaying type of memory.

Very often, it is useful to analyze the process in the Fourier space. In this space, the counterpart of the autocovariance is the power spectral density (psd), which we define as [15]

$$\mathrm{psd}_X(\omega) := \sum_{k=-\infty}^{\infty} \mathrm{acov}_X(k) \mathrm{e}^{-\mathrm{i}\omega k}. \tag{12}$$

The well-known formula for the Fourier-transform of the geometric sequence yields that, for the AR(1) process, the psd reads [15,16]

$$\mathrm{psd}_X(\omega) = \frac{\sigma^2}{1 + a^2 - 2a\ \cos(\omega)}. \tag{13}$$

The psd of a recorded time series can be estimated using various methods based on numerical Fourier-transform of data. Here, we use the smoothed periodogram, a very popular and thoroughly studied estimator [15,17]. The time series itself does not contain information about the physical time scale, so the periodogram is calculated in normalized, dimensionless units in which the sampling frequency is one. However, the psd is a function symmetric with respect to $\omega = 0.5$, so we only estimate its values in the interval [0,0.5].

A comparison of the estimated psd with the one corresponding to the AR(1) model (13) and calculated for the estimated $\hat{a}$, shows essential dissonance between these two for the high-frequency recording (see Fig. 2). Unfortunately, it is difficult to find a source of this effect only from analysis of the psd. To show the origin of this effect, the partial autocorrelation function must be used.

4. Partial Autocorrelation Analysis

Partial autocorrelation $\mathrm{pacf}_X(k)$ of the stationary series is the memory function, measuring a dependence between X_i and X_{i+k} (it does not depend on choice of index i), with influences from in-between X_j, $i < j < i + k$ removed [14,15]. This removal is performed by subtracting the projections (in the Hilbert space sense) onto the subspace of variables $X_{i+1}, \ldots, X_{i+k}$, and denoted $\mathcal{P}_{X_{i+1},\ldots,X_{i+k-1}}$. The definition of the $\mathrm{pacf}_X(k)$ reads explicitly:

$$\mathrm{pacf}_X(k) := \mathrm{corr}(X_i - \mathcal{P}_{X_{i+1},\ldots,X_{i+k-1}}(X_i), X_{i+k} - \mathcal{P}_{X_{i+1},\ldots,X_{i+k-1}}(X_{i+k})), \tag{14}$$

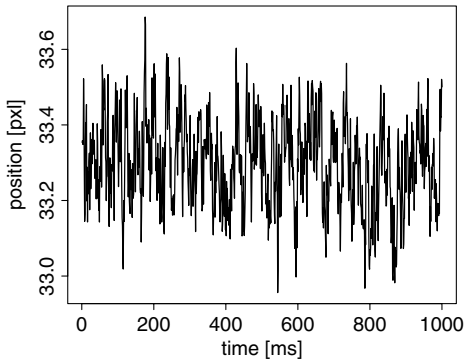

Fig. 1. Plot of an exemplary trajectory recorded with sampling frequency 5000 fps (1000 measurements).

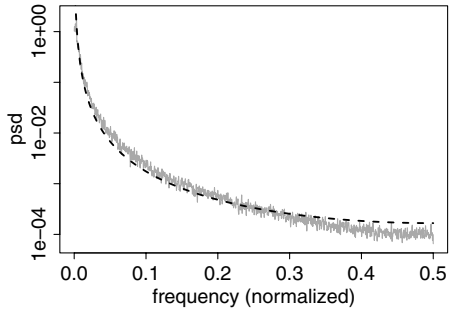

Fig. 2. Estimate of the psd (gray line) and the fitted AR(1) psd (dashed black line) for recording made with sampling frequency 10^4 fps.

where we additionally use the convention that $\mathcal{P}_{\varnothing} = 0$.

The partial autocorrelation is a useful function, because removing these projections, we somewhat get rid of the influence of the time evolution between moments i and j. This procedure helps clarify the analysis of the memory. The pacf is a measure of only direct dependence between the values of the studied process. To illustrate this point, let us derive the pacf of the AR(1) process. The definition $X_n = aX_{n-1} + \xi_n$ immediately suggests that X_n directly depends only on X_{n-1}, and this dependence has strength a. This observation can be easily supported by more strict reasoning. The subspace generated by $X_{i+1}, \ldots, X_{j-1}$ is the same as the subspace generated by $X_{i+1}, \xi_{i+2}, \ldots, \xi_{j-1}$. The projection on the latter can be performed in a straightforward manner using Eq. (8). After subtracting the projection, X_j reduces to ξ_j, which is orthogonal to every past value X_i. This supports the intuitive result that, for the AR(1) process,

$$\mathrm{pacf}_X(k) = \begin{cases} 1, & k = 0; \\ a, & k = 1; \\ 0, & k > 1. \end{cases} \tag{15}$$

The partial autocorrelation can be estimated using the Yule–Walker equations, which relate it to the autocovariance [15]. This set of equations can be easily solved numerically. For our data, the pacf for low frequencies fits to the model (see Fig. 3). By two dashed lines near zero we denote the level of an expected statistical error. Values between these lines are statistically insignificant.

However, the high-frequency data have pacf of a different type (see Fig. 4). It looks like a geometric series with a negative rate, which indicates the proper adjustment of the model.

5. Adjusted Model: ARMA(1,1) Process

It appears that a proper modification explaining the data is addition of the first-order moving average MA (1) part to the AR(1) model. The MA(1) part represents a process for which the present value depends linearly on one past value of the external noise (not the process itself), i.e., $\xi_n + b\xi_{n-1}$ [14,15]. The

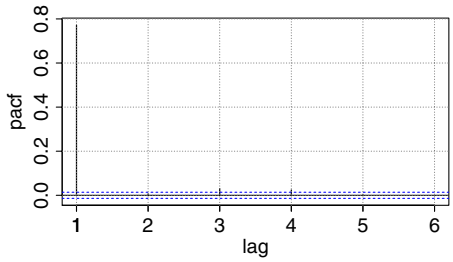

Fig. 3. Partial autocorrelation estimated from the bead's trajectory for low-frequency sampling at 10^3 fps.

complete model, with both AR(1) and MA(1) parts, is called ARMA(1,1), and explicitly is expressed as

$$X_n = aX_{n-1} + \xi_n + b\xi_{n-1}. \tag{16}$$

Unfortunately, from this form it is not clear what is the direct dependence between X_n and the past values of the process, because ξ_{n-1} is not orthogonal to these values. However, using the identity $X_{n-1} = aX_{n-2} + \xi_{n-1} + b\xi_{n-2}$, we may write $\xi_{n-1} = X_{n-1} - aX_{n-2} - b\xi_{n-2}$. Substituting this equality into Eq. (16), we obtain

$$X_n = (a+b)X_{n-1} - abX_{n-2} - b^2\xi_{n-2}. \tag{17}$$

Now, we may repeat this procedure using the identity for ξ_{n-2} and the above formula. Continuing recursively, we obtain

$$X_n = (a+b)\sum_{k=1}^{\infty}(-b)^{k-1}X_{n-k}. \tag{18}$$

This formula shows the explicit form of dependence between X_n and the past values X_{n-k}, therefore justifying why the partial autocorrelation has the form of a geometric series fitting the behavior of the analyzed data. The parameters a and b can be estimated using least squares or maximum likelihood techniques [14,15]. Performed fit returned $\hat{b} = 0.212 \pm 0.005$ and $\hat{a} = 0.976 \pm 0.001$, which corresponds perfectly to the ARMA(1,1) process with the pacf, drawn in Fig. 4. The given uncertainties of $\hat{a}$ and $\hat{b}$ are standard deviations, estimated from a sample of ten trajectories with 60,000 observations in each. The obtained sample of ten estimates of a can be considered Gaussian on a standard level of significance 0.05 by

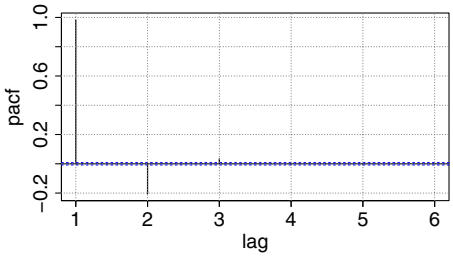

Fig. 4. Partial autocorrelation estimated from the bead's trajectory for high-frequency sampling at 10^4 fps.

Shapiro–Wilk, Anderson–Darling, and Pearson χ^2 tests, and the same is true for b. This agrees with the well-known theory of long-trajectory asymptotics of the used estimators [14]. These standard deviations are only slightly greater than the deviations for these estimators for such an ARMA(1,1) process (which was checked by Monte Carlo simulation). This means that measurement imperfections do not distort the precision of estimation.

Of course, there is no possibility to rule out that performed estimation is precise, although biased. However, note that the obtained value $\hat{a}$ is consistent with the measurements of the stiffness for lower frequencies.

The ARMA(1,1) can be naturally explained as an influence of the high-frequency CCD camera. When the frequency of the sampling is high, the CCD matrix has no time to fully refresh between subsequent photos. The remainder of the last frame is still visible on the current one (the recording is smudgy and blurred), which causes the center of the mass position X_n to include part of the value X_{n-1} from the last frame. Instead of X_n, we observe $X'_n = X_n + bX_{n-1}$. Parameter b is exactly the amount of intensity left from the last frame on the actual one, $0 < b < 1$. In this situation,

$$\begin{aligned} X'_n &= X_n + bX_{n-1} \\ &= a(X_{n-1} + bX_{n-2}) + \xi_n + b\xi_{n-1} \\ &= aX'_{n-1} + \xi_n + b\xi_{n-1}, \end{aligned} \tag{19}$$

so X'_n is the ARMA(1,1) process. It is straightforward to obtain the autocovariance of this new process as

$$\begin{aligned} \mathrm{acov}_{X'}(k) &= \mathrm{cov}(X_n + bX_{n-1}, X_{n+k} + bX_{n-1+k}) \\ &= (1+b^2)\mathrm{acov}_X(k) + b\mathrm{acov}_X(k-1) \\ &\quad + b\mathrm{acov}_X(k+1). \end{aligned} \tag{20}$$

As we can see, the autocovariance is the sum of three geometric sequences. The form of the revised psd follows from the linearity of the Fourier-transform:

$$\mathrm{psd}_X(\omega) = \sigma^2 \frac{1 + b^2 + 2b\,\cos(\omega)}{1 + a^2 - 2a\,\cos(\omega)}. \tag{21}$$

This revised psd fits the data perfectly (see Fig. 5). Hence, the ARMA(1,1) in the case of high-frequency recordings describes better the experimental data than the commonly used AR(1) model.

6. Influence of the Exposure Time

The previous considerations prove the utility of the ARMA(1,1) model; however, they do not imply that the observed effect is due to the influence of the CCD camera. To justify our claim, we provide further experimental evidence. During all our previous measurements, the exposure time for taking a frame was 45 μs. The longer exposition is, in most situations,

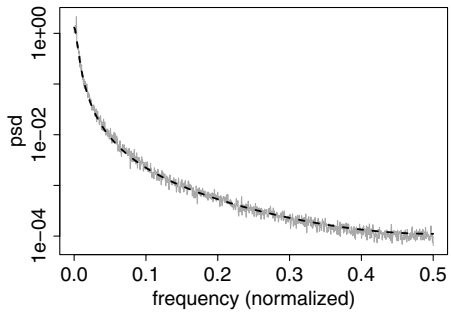

Fig. 5. Estimate of the psd (gray line) and the fitted ARMA(1,1) psd (dashed black line).

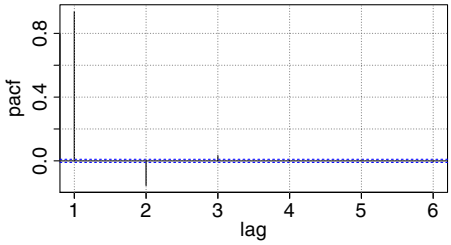

Fig. 6. Estimated pacf of trajectory taken with frequency of sampling 10^3 fps, but exposure time increased to 895 μs.

used only when necessary (e.g., in cases of low illumination), since the recording becomes more blurred. Therefore, if our conclusion is correct, then an increase of the exposition time would incorporate an MA(1) part, even for low frequencies. This indeed is true, as seen in Fig. 6 and compared with Figs. 3 and 4.

The obtained effect is identical to the MA(1) part (with coefficient $\hat{b} = 0.172 \pm 0.005$) present for high-frequency and low exposure time data. An analogical operation, performed for larger sampling frequencies, increases the value of the MA(1) coefficients. Unfortunately, a decrease of the exposition, which would likely diminish the MA(1) part for higher frequencies, is hard to obtain for technical reasons, which leaves the described methodology as the only practical way to deal with this influence.

7. Summary

We have shown that the high-frequency CCD camera influences the recorded time series of positions of a bead trapped in optical tweezers. By adding of the MA(1) part to the classical AR(1) model, we have obtained full agreement with the recorded data. The proposed ARMA(1,1) model allows for a better understanding of the tweezers' dynamics. We suggest that the studied effect, which we explain by the slow refreshment rate of the CCD matrix, has to be included in more advanced studies, such as the interactions of the optical tweezers with diverse complex environments. We hope that this insight is a substantial advance in the statistical analysis within this area. Moreover, we stress that the described statistical methods are simple to use by nonstatisticians and already implemented in many scientific environments, such as R-package and MATLAB.

The work of S. D. was supported by the Polish Ministry of Scientific Research and Information Technology Grant No. N N518 498839. The work of J. Ś. was partially supported by National Science Centre Poland Maestro Project No. 2012/06/A/ST1/00258.

References

1. K. C. Neuman and S. M. Block, "Optical trapping," Rev. Sci. Instrum. **75**, 2787–2809 (2004).
2. A. Ranaweera, *Investigations with Optical Tweezers: Construction, Identification, and Control* (University of California, 2004).
3. L. P. Ghislain, N. A. Switz, and W. W. Webb, "Measurement of small forces using an optical trap," Rev. Sci. Instrum. **65**, 2762–2768 (1994).
4. M. D. Wang, H. Yin, R. Landick, J. Gelles, and S. M. Block, "Stretching DNA with optical tweezers," Biophys J. **72**, 1335–1346 (1997).
5. S. B. Smith, Y. Cui, and C. Bustamante, "Overstretching B-DNA: the elastic response of individual double-stranded and single-stranded DNA molecules," Science **271**, 795–799 (1996).
6. M. E. Arsenault, Y. Sun, H. H. Baua, and Y. E. Goldman, "Using electrical and optical tweezers to facilitate studies of molecular motors," Phys. Chem. Chem. Phys. **11**, 4834–4839 (2009).
7. A. D. Mehta, M. Rief, J. A. Spudich, D. A. Smith, and R. M. Simmons, "Single-molecule biomechanics with optical methods," Science **283**, 1689–1695 (1999).
8. D. G. Grier, "Optical tweezers in colloid and interface science," Curr. Opin. Colloid Interface Sci. **2**, 264–270 (1997).
9. W. Coffey, Yu. Kalmykov, and J. Waldron, *The Langevin Equation* (World Scientific, 2005).
10. K. Sobczyk, *Stochastic Differential Equations* (Kluwer Academic, 1991).
11. D. Grier and Y. Roichman, "Holographic optical trapping," Appl. Opt. **45**, 880–887 (2006).
12. M. Polin, K. Ladavac, S.-H. Lee, Y. Roichman, and D. G. Grier, "Optimized holographic optical traps," Opt. Express **13**, 5831–5845 (2005).
13. A. Horst and N. Forde, "Power spectral analysis for optical trap stiffness calibration from high-speed camera position detection with limited bandwidth," Opt. Express **18**, 7670–7677 (2010).
14. P. Brockwell and R. Davis, *Time Series: Theory and Methods* (Springer-Verlag, 2006).
15. G. Box, G. Jenkins, and G. Reinsel, *Time Series Analysis: Forecasting and Control* (Prentice-Hall, 1994).
16. K. Berg-Sørensen and H. Flyvbjerg, "Power spectrum analysis for optical tweezers," Rev. Sci. Instrum. **75**, 594–613 (2004).
17. S. J. Orfanidis, *Introduction to Signal Processing* (Prentice-Hall, 1995).